Asian Journal of Advanced Research and Reports

7(4): 1-18, 2019; Article no.AJARR.53390
ISSN: 2582-3248

Soccer Ball Spatial Kinematics and Dynamics Simulation for Efficient Sports Analysis

Ying Li[1*] and Qi Li[2]

[1]Department of Mining Engineering, University of Missouri-Rolla, Missouri, USA.
[2]Primary and High School, North University of China, Taiyuan, Shanxi, China.

Authors' contributions

This work was carried out in collaboration between both authors. Author YL performed the modeling, simulation and analysis, managed the literature searches, wrote the protocol and wrote the first draft of the manuscript. Author QL designed the geometric model and performed animation analysis. Both authors read and approved the final manuscript.

Article Information

DOI: 10.9734/AJARR/2019/v7i430184
Editor(s):
(1) Dr. Shu-Lung Kuo, Associate Professor, Engineering Consultant, Kelee, Environmental Consultant Corporation, Kaohsiung City, Taiwan and Department of Technology Management, the Open University of Kaohsiung, Kaohsiung City, Taiwan.
Reviewers:
(1) Adel H. Phillips, Ain-Shams University, Abbasia, Cairo, Egypt.
(2) Solomon Omwoma, University of Science and Technology, Kenya.
(3) Abdul Samad Khan, Northwestern Polytechnical University, Xian, P. R. China.
Complete Peer review History: http://www.sdiarticle4.com/review-history/53390

Original Research Article

Received 15 October 2019
Accepted 20 December 2019
Published 25 December 2019

ABSTRACT

The intelligent sports analysis requires exactly modeling the kinematics and dynamics of a soccer ball in a three-dimensional (3D) space. To address this problem, a 3D dynamic model of the soccer ball is developed to simulate the motion and capture the kinematics and dynamics performance. The model consists of three sub-models governed by the classic mechanics and formulated as time-dependent ordinary differential equations (ODEs). The simulations involve visualizing the ball traveling trajectory, which contains the instantaneous force information; and plotting the time-varying displacement and force curves. The model is validated by comparison of the results from this simulation and another theoretical calculation. A case study is presented to simulate the projectile motion of a soccer ball in a virtual environment. The spatial kinematics and dynamics results are obtained and analyzed. The results show the max projectile height and range, and kick force increase with the increase of the initial velocity. This research is significant to simulate the soccer ball motion for promoting the planning, evaluation, and optimization of trajectory.

**Corresponding author: Email: liyinglzh@yahoo.com;*

Keywords: Soccer ball; dynamics model; virtual simulation; model validation; kinematics analysis; dynamics analysis.

1. INTRODUCTION

Dynamics model of a soccer ball can help to carry out the trajectory planning without practicing on a field; and dynamic simulation can accurately represent the motion of the ball to capture its dynamics performance to achieve force, trajectory, and position optimization.

The researches of a soccer ball motion focus on mathematical modeling, computer simulation, and experimental measurement. In the early time, some physics or dynamics textbooks [1,2,3], already use a soccer ball projectile motion as an example to teach how to solve the particle kinematics problem in two dimensions (2D). Equation of motion is created as a simple ordinary differential equation (ODE). The external force involved in the equation is only gravity. With given a launching speed and an initial angle, the projectile trajectory is found.

Following this fundamental mathematical model, the moving trajectories of a soccer ball are widely investigated by considering some environmental factors and initial conditions. Typically, the air resistance (aerodynamic drag) has been added in the equation of motion [4,5]. The effect of air resistance on the trajectory has been discussed. The results show that air resistance is a very important factor in understanding the motion of fast-moving soccer ball. It depends on not only the size, shape, surface roughness of a ball, but also the boundary layer: the laminar flow or turbulence. In some experimental studies [6,7,8,9], the drag coefficients are suggested for accounting the effect of the boundary layer on the drag of a soccer ball.

The above research and development build a solid foundation to further investigate the motion of any kind of flight object. For example, the effects of the projectile angle on a particle traveling trajectory, velocity, and acceleration are studied using the equation of motion with consideration of air resistance [10]. Additionally, the effects of initial velocity, kick force, and kick position on the projectile trajectory of a soccer ball are explored [11,12,8].

Reviewing previous researches brings some new considerations. The 2D soccer ball model is overly simplified by neglecting its three-dimensional (3D) characteristics. For instance, in reality, the air resistance is a complex spatial force due to the variation of wind direction. Its boundary layer can transition from laminar flow to turbulence. It requires for full spatial representation of resistance to accurately demonstrate its spatial trajectory and capture its instantaneous position. This kind of consideration promotes to extend the study to the general, 3D case, which allows the formulation of a full dynamic simulation of a soccer ball.

Recently, a training system is designed to simulate the free-kick of a soccer ball. The trajectory can be predicted for the given initial parameters [13]. The study has focused on the kinematics simulation rather than the dynamics simulation. Therefore, the contact force of the ball-ground doesn't include in their model. The dynamic forces applied to the ball are not mentioned. The study emphasizes system development instead of sports analysis. The model validation is neglected. The detailed analysis and discussion are not given in the simulation results.

In this study, a spatial kinematics and dynamics model of a soccer ball is developed. The model allows randomly applying a kick force or initial velocity on the ball in 3D space. The air resistance applied on the ball is formulated in x-y-z directions. And, the equation of the contact force between the ball and ground is integrated into the model. The model is validated by a comparison of this simulation result and a theoretical calculation result [10]. An example is presented for demonstrating the model application as well as kinematics and dynamics analysis.

2. DYNAMICS MODEL OF A SOCCER BALL PROJECTILE MOTION

In this section, a dynamics model is built for the dynamic simulation of a soccer ball projectile motion. The model consists of several groups of mathematical equations, which are the equation of foot-ball impulsive force, the equations of ball projectile motion, the equations of air resistance applied on the ball, and the equations of ball-ground contact at the landing point. The model is created by ignoring the ball flying spin, Magnus effect, and gyroscopic moment [7,10]. The modeling details are given in the following three aspects.

2.1 Equations of Soccer Ball Impulsive Force

Fig. 1 shows a diagram of the initial configuration of foot-ball contact. A ball with mass m is moving at a velocity $\vec{v}_1$ on a given direction and is kicked by a player by an impulsive force $\vec{P}$. When the ball leaves the player's foot, the ball travels with an initial shooting velocity $\vec{v}_2$ ($\vec{v}_0$) at an initial projectile angle θ_0, and initial orientation angle β_0. If the foot and ball are in contact with time Δt, the relationship between the force vector $\vec{P}$ and velocity vectors $\vec{v}_1$ and $\vec{v}_2$ can be given by the principle of linear impulse and momentum [1] as illustrated in Equation 2.1.

$$\vec{P}\Delta t = (m\vec{v})_2 - (m\vec{v})_1 \quad (2.1)$$

$$\vec{P} = \frac{(m\vec{v})_2 - (m\vec{v})_1}{\Delta t} \quad (2.1a)$$

$$\vec{v}_2 = \frac{\vec{P}\Delta t + (m\vec{v})_1}{m} \quad (2.1b)$$

Usually, two problem-solutions are paid attention to (i) given velocities $\vec{v}_1$ and $\vec{v}_2$ to find the magnitude, and direction of the average impulsive force $\vec{P}$ (see Equation 2.1a); and (ii) reversely, given impulsive force $\vec{P}$ and $\vec{v}_1$ to find the magnitude and direction of $\vec{v}_2$ (see Equation 2.1b). In the next sub-section, the $\vec{v}_2$ will take a role as an initial velocity $\vec{v}_0$ to shoot the ball and let it travel with projectile motion.

2.2 Dynamic Equations of Soccer Ball Projectile Motion

Fig. 2 shows a soccer ball projectile motion through the air on a field. A Cartesian coordinate system o(x, y, z) is attached to the field ground at the ball center of mass in initial position, where x-z plane attached on the soccer field with x-axis along the length direction and z-axis along the width direction, as well as y-axis is perpendicular to the x-z plane. Initial velocity vectorv ⃗0 of the

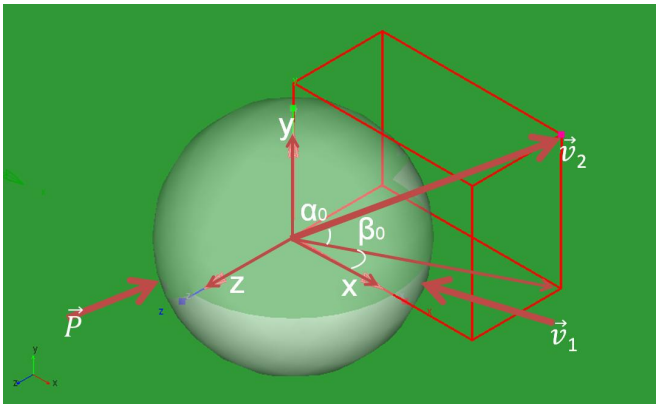

Fig. 1. Initial configuration for a soccer ball projectile motion

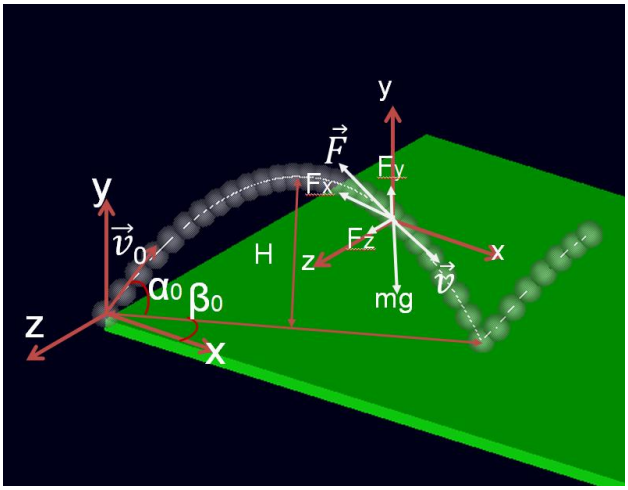

Fig. 2. A soccer ball projectile motion with the free-body diagram at an instantaneous position

ball related to the initial projectile angle θ_0, and initial orientation angle β_0 can be broken down into three scalar components v_{x0}, v_{y0}, and v_{z0} in x-y-z directions as illustrated in Equations 2.2-2.4.

$$v_{x0} = v_0 \cos\theta_0 \cos\beta_0 \quad (2.2)$$
$$v_{y0} = v_0 \sin\theta_0 \quad (2.3)$$
$$v_{z0} = -v_0 \cos\theta_0 \sin\beta_0 \quad (2.4)$$

When the ball travels through the air, the air resists the ball motion with resistance $\vec{F}$. It depends on the density of the air ρ, the cross-sectional area of the ball A, the velocity of the ball moving $\vec{v}$ and the drag coefficient C_d. The drag coefficient depends on the boundary conditions, such as the surface roughness of a ball, as well as the laminar flow or turbulence of the atmospheric layer. The drag coefficients of a soccer ball are suggested between 0.1 and 0.5 [9,14]. Then, the force of air resistance is established as Equations 2.5 and 2.6 [6,7,8,4].

$$\vec{F} = -\frac{1}{2}\rho C_d A \vec{v}[\vec{v}] = -K\vec{v}|\vec{v}| \quad (2.5)$$

If d denotes the diameter of the ball, then

$$K = \frac{1}{8}\rho C_d \pi d^2 \quad (2.6)$$

Fig. 2 also shows a free-body diagram of the ball in an instantaneous position. It notes that air resistance $\vec{F}$ is aligned and opposite to the velocity $\vec{v}$ direction. K is related to density, drag, and area. If the air resistance is non-homogenous, K is broken down into three components K_x, K_y, and K_z along with x-y-z directions, respectively. Vector Equation 2.5 can be represented as three sets of scalar Equations 2.7-2.9 to calculate the component resistance forces F_x, F_y and F_z, which are applied to the ball in x-y-z directions, respectively.

$$F_x = -K_x\dot{x}|\dot{x}| \quad (2.7)$$
$$F_y = -K_y\dot{y}|\dot{y}| \quad (2.8)$$
$$F_z = -K_z\dot{z}|\dot{z}| \quad (2.9)$$

With the assumption that only air resistance F and gravity mg applied on the ball, the general motion Equation 2.10 is derived by Newton's Second Law [15].

$$\sum \vec{N} = m\vec{a} \quad (2.10)$$

where $\sum \vec{N}$ is the vector of general external force, and $\vec{a}$ is the acceleration vector of the ball. Based on the free-body diagram in Fig. 2, Equation 2.10 is separated into the following three sets of scalar Equations 2.11-2.13 for calculating x-y-z component motions, respectively.

$$m\ddot{x} + K_x\dot{x}|\dot{x}| = 0 \quad (2.11)$$
$$m\ddot{y} + K_y\dot{y}|\dot{y}| + mg = 0 \quad (2.12)$$
$$m\ddot{z} + K_z\dot{z}|\dot{z}| = 0 \quad (2.13)$$

The combined Equations 2.2-2.4 and 11-13 form a kinematics and dynamics system to simulate the ball projectile motion. Considering the initial conditions (Equations 2.2-2.4), ODEs 2.11-2.13 can be solved to find displacements, velocities, accelerations, and forces for generating expected trajectory.

2.3 Equations of Motion for Ball-ground Contact System

When the ball lands on the ground, the ball impacts the ground and finishes the projectile motion. Fig. 3 shows a diagram of the final configuration of ball-ground contact. That is a ball-ground contact model, which is created as a mass-spring-dashpot system [16] with one degree of freedom to generate the interaction between the ball and ground. The mass m is equal to the mass of the ball, the spring represents the ball's elastic properties and the dashpot expresses the balls damping characteristics. There are three types of forces applied to the system, internal forces, external forces, and inertia force.

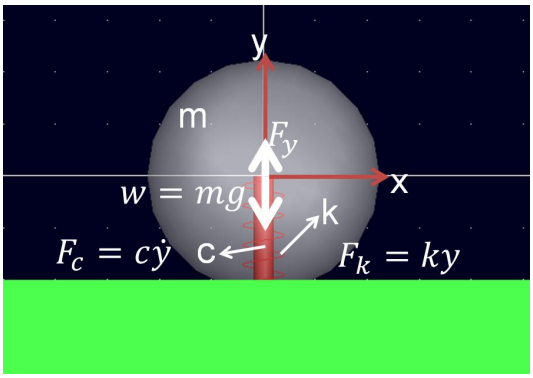

Fig. 3. A ball-ground contact model with a mass-spring-dashpot system

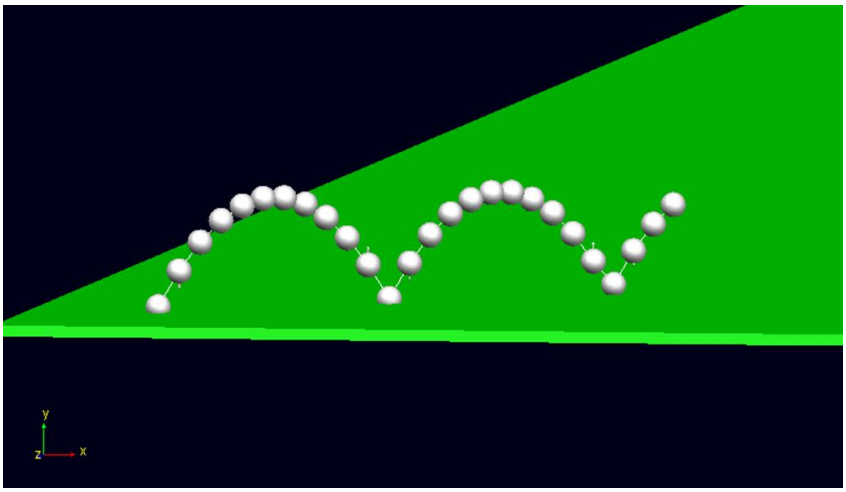

Fig. 4. An animation result of the projectile motion trajectory of a soccer ball

The internal forces are caused by the spring and damping, which act in the y-direction of contact normal at the ball-ground contact patch. This normal reaction force has two components, a spring force F_k, which is proportional to stiffness k and deflection, and opposite to the relative deflation; and a damping force F_c, which are proportional to the damping coefficient c and the rate of deflation, and opposite to the direction of relative motion.

The external forces come from gravity w and y-air resistance F_y (see Equation 2.8), which are applied to the ball in the y-direction.

The inertia force is related to the mass of the ball and the acceleration of deflation, which is also applied to the ball in the y-direction.

Employing Newtown's Second Law (Equation 2.10), the equation of motion for the ball-ground contact is given by Equations 2.14 and 2.15.

$$m\ddot{y} = \sum N_y = F_c + F_k - W + F_y \qquad (2.14)$$

$$m\ddot{y} = c\dot{y} + ky - mg + K_y\dot{y}|\dot{y}| \qquad (2.15)$$

It notes that Ordinary Differential Equation 2.15 combines the relative motion, damping, and stiffness.

The integration of three sub-models established in Sections 2.1-2.3 builds a dynamics simulation system for capturing kinematics and dynamics performance of a soccer ball projectile motion. Using a tool of dynamics software [11], it can solve problems from impulsive force Equation 2.1 through projectile motion Equations 2.11-2.13 to ball-ground contact Equation 2.15. The animation results visualize the projectile trajectory of a soccer ball as demonstrated in Fig. 4. The numerical results give the time-varying impulsive force of the foot-ball, projectile motion (displacements, velocities, accelerations), and contact forces of the ball-ground.

The solution for these models supports the sports analysis of soccer ball. The dynamics models can help players to find the kicking force, kicking position and kicking angle to achieve an expected trajectory. The dynamic simulation can be used to the motion and dynamic force analysis for training players.

3. VALIDATION OF THE SOCCER BALL PROJECTILE MOTION MODEL

The proposed dynamics model of a soccer ball projectile motion is validated by comparing the results of the motion simulation obtained from this research against those from a mathematical model reported by Hroncová and Grieš [10]. The comparison results of displacement simulation in a 2D Cartesian coordinate system o(x, y) between two models are shown in Figs. 5 and 6, respectively. The details are discussed in the following two aspects.

Firstly, a soccer ball projectile motion is simulated using the dynamics model created in this research. For comparing purpose, the parameters, such as initial conditions and simulation time are selected as same as those

used in a case study reported by Hroncová and Grieš [10]. They are: the mass of the ball m=0.43 kg, initial projectile angle θ_0=45°, initial orientation angle β_0=0°, initial velocity v_0=46.5 m/s and air resistance coefficient K=0.00002 kg/m. Two solid black lines in Figs. 5 and 6 indicate the simulation results of the soccer ball projectile motion along the x-axis and y-axis during the time of 7 seconds (s). Fig. 5 describes the ball displacement along the x-axis (black solid line) and Fig. 6 does the displacement along the y-axis (black solid line).

Secondly, Hroncová and Grieš [10] establish a mathematical model of a particle moving in x-y space within the air resistance environment integrating classic mechanics and aerodynamics. The motions of the particle projectile in the horizontal x-direction and vertical y-direction are given as Equations 3.1 and 3.2, respectively.

$$x = \frac{v_0}{k_1}\cos\theta_0(1 - e^{-k_1 t}) \tag{3.1}$$

$$y = \frac{g + v_0 k_1 \sin\theta_0}{k_1}(1 - e^{-k_1 t}) - \frac{g}{k_1}t \tag{3.2}$$

where v_0 is the particle initial velocity, θ_0 is the particle initial projectile angle, $k_1 = F/mv$, F is the air resistance, m is the particle mass, and v is the velocity of the particle.

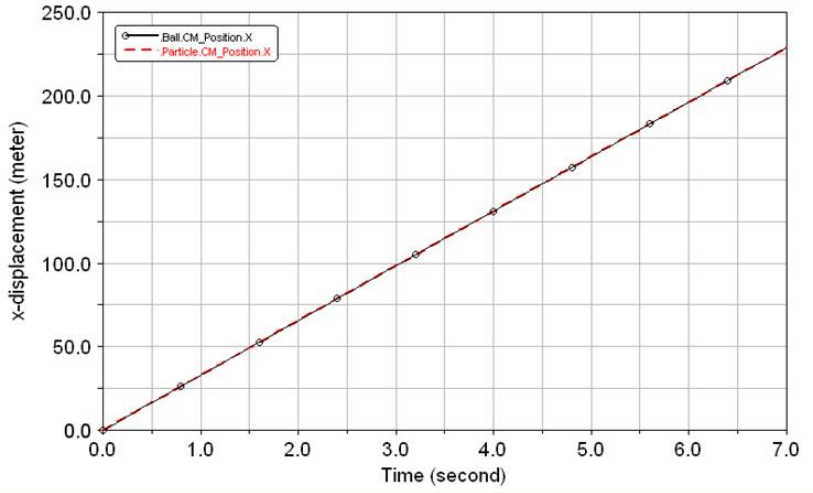

Fig. 5. Comparison of projectile displacements in the x-direction from the simulation and calculation results versus time 7 seconds

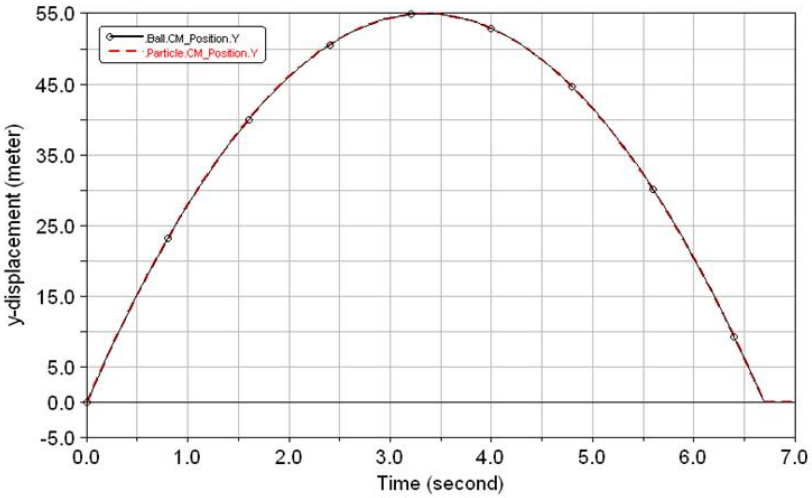

Fig. 6. Comparison of projectile displacements in the y-direction from the simulation and calculation results versus time 7 seconds

In their article, a case study is conducted using Equations 3.1 and 3.2 to find a particle displacement versus time in a Cartesian coordinate system o(x, y). Initial conditions are set as: θ_0=45°, and v_0= 46.5 m/s. The calculation results are given as two red dash lines in Figs. 5 and 6. In Fig. 5, the red dash line represents the particle displacement in x-direction within the time of 7s; and in Fig. 6, the red dash line represents the particle displacement in y-direction within the time of 7s.

In Figs. 5 and 6, it notes that even though the simulation and calculation results are conducted using two different models from two different teams, the x or y displacement results compare favorably with each other. Therefore, there is no difference between the simulated x-y displacements and calculated x-y displacements. No matter what kind of result it is, the x-displacement almost linearly increases from 0 to 219 m within the time range of 0-6.7s as shown in Fig. 5. The y-displacement shows a parabolic shape, which increases from 0 to 55 m within 0 to 3.4s and then decreases from 55 to 0 m within 3.4 to 6.7s as shown in Fig. 6. It is important to note that the max projectile length is 219 m and the max projectile height is 55 m.

This analysis case validates the potential of the dynamics model to predict a soccer ball projectile motion with air resistance. The analysis results identify that the dynamics simulation will give a higher confidence in the soccer ball kinematics simulation with the consideration of the air resistance. The analysis results also illustrate that the dynamics model can capture the ball projectile motion such as the horizontally shooting range (x-displacement) and vertically shooting high (y-displacement). Anyway, for the 3D dynamics model created in this research, it can also capture the motion in the z-direction.

In reality, a soccer ball kicked by a player will not be expected to shoot at such a great speed of 46.5 m/s and move so far away from 219 m. The moving direction of the ball can be random in 3D space instead of 2D space because a player can choose to kick at any position and orientation around the ball. For addressing these issues, a case study is demonstrated in the next section.

4. ONE CASE STUDY OF A SOCCER BALL PROJECTILE MOTION

In this case study, using the developed dynamics model as shown in Fig. 7, a soccer ball projectile motion through the air is simulated in a Cartesian coordinate system o(x, y, z), where x-z plane attached on the soccer field with x-axis along the length direction and z-axis along the width direction, as well as y-axis is perpendicular to the x-z plane.

The geometric parameters are selected as: a virtual soccer field is sized in the length of 120 m and width of 90 m. The mass of the ball m=0.43 kg, its diameter d=0.2286 m, sea level static density ρ=1.221 kg/m^3, and drag coefficient C_d=0.25 [9].

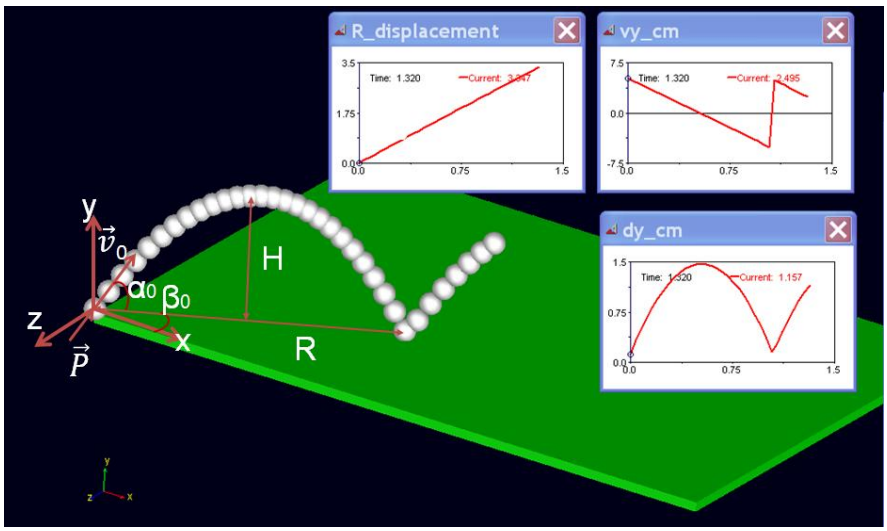

Fig. 7. A soccer ball dynamics model

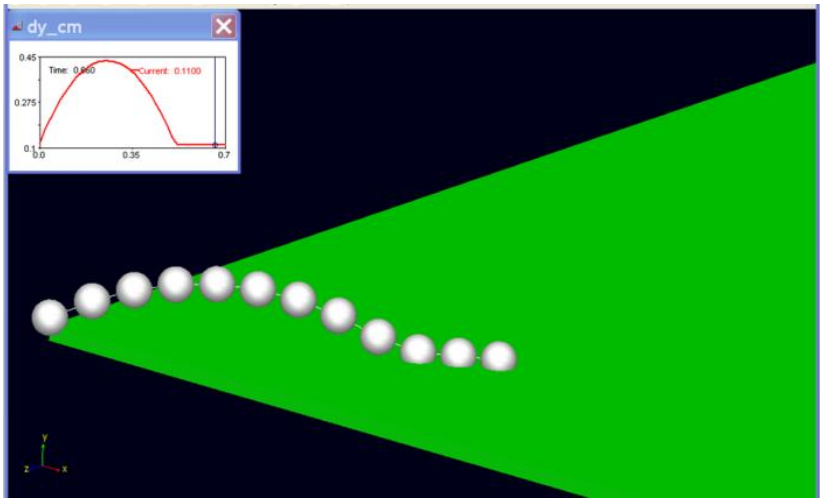

(a) Initial velocity v_0=5 m/s

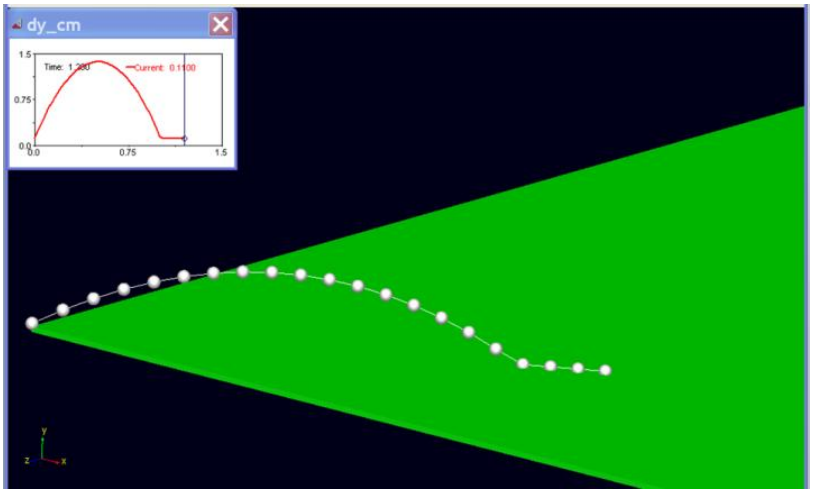

(b) Initial velocity v_0=10 m/s

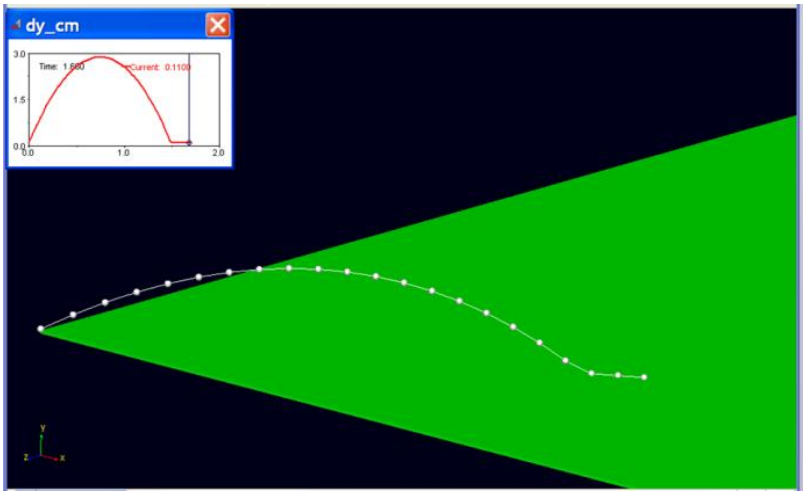

(c) Initial velocity v_0=15 m/s

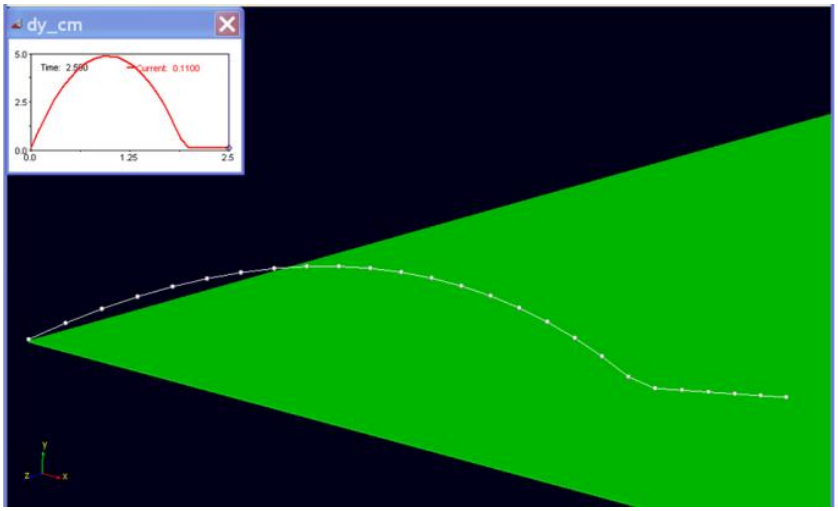

(d) Initial velocity v_0=20 m/s

Fig. 8. A soccer ball projectile motion with four initial velocities

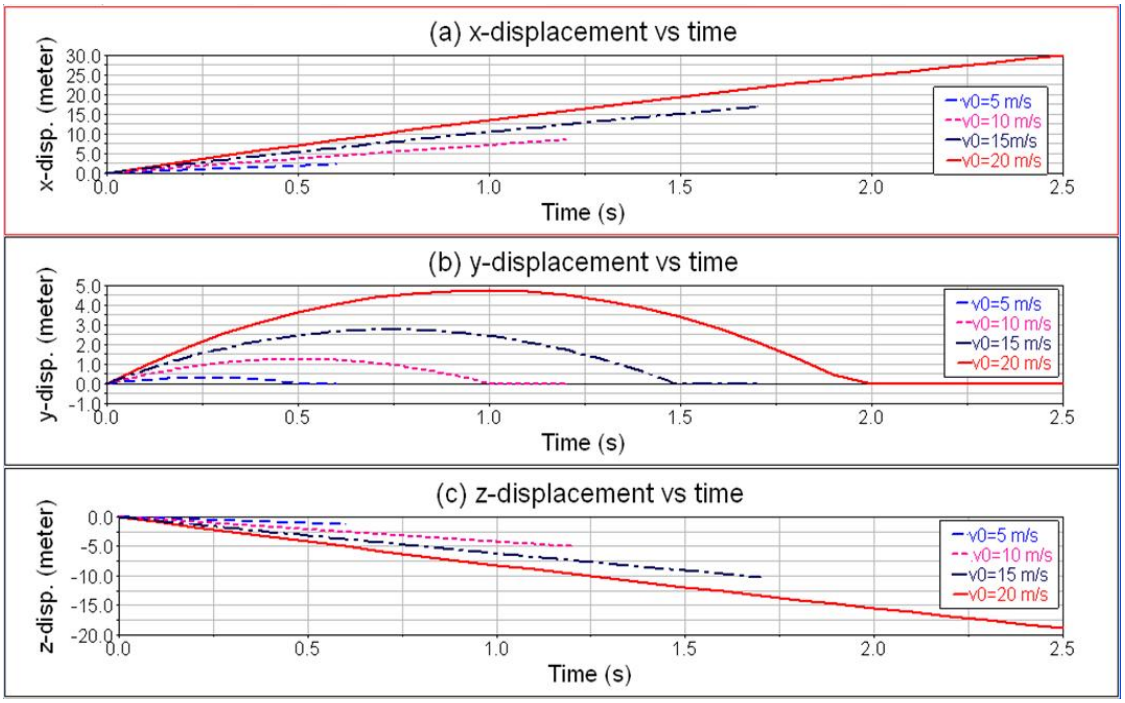

Fig. 9. Numerical results of a soccer ball displacements in x-y-z directions with four initial velocities v_0= 5, 10, 15 and 20 m/s

The initial conditions are: a soccer ball is initially at rest on the ground and kicked with an impulsive force $\vec{P}$. The ball is shot with an initial velocity v_0 at an initial projectile angle θ_0=30°, and an initial orientation angle β_0=30°. The air resistance is homogenous.

Since the air resistance is homogenous, air resistance coefficient K=0.00622 kg/m, which is calculated by Equation 2.6. Equations 2.7-2.9 are simplified to Equations 4.1-4.3 to calculate the component resistance forces F_x, F_y and F_z, which are applied to the ball in x-y-z directions, respectively.

$$F_x = -K\dot{x}^2 \quad (4.1)$$

$$F_y = \mp K\dot{y}^2 \quad (4.2)$$

$$F_z = K\dot{z}^2 \quad (4.3)$$

In Equation 4.2, the sign "$\mp$" depends on the ball motion: the negative sign "-" for the ball moving up; and the positive sign "+" for the ball moving down.

Motion Equations 2.11-2.13 are simplified to Equations 4.4-4.6, respectively.

$$m\ddot{x} + K\dot{x}^2 = 0 \quad (4.4)$$

$$m\ddot{y} \pm K\dot{y}^2 + mg = 0 \quad (4.5)$$

$$m\ddot{z} + K\dot{z}^2 = 0 \quad (4.6)$$

In Equation 4.5, the sign "$\pm$" depends on the ball motion: the positive sign "+" for the ball moving up; and the negative sign "-" for the ball moving down.

Kinematics and dynamics simulations are conducted with the selected four groups of times. The moving trajectories of the ball are visualized in a virtual soccer environment. The dynamic displacements and forces are measured by assigning four initial velocities v_0=5, 10, 15, and 20 m/s, respectively. Some significant kinematics and dynamics results are obtained and analyzed.

4.1 Kinematics Simulation and Analysis

Fig. 8a-d exhibits the animation results of the soccer ball projectile motion with four initial velocities v_0=5, 10, 15, and 20 m/s responding to four times 0t=0.65, 1.2, 1.7, and 2.5 s, respectively. It notes that four trajectories all show parabolic shapes. And also, the bigger the initial velocity, the higher the ball reaches, and the farther the ball shoots. Fig. 9a-c reveals the numerical results of the instantaneous position of the ball traveling in x-y-z directions with four initial velocities v_0 =5, 10, 15, and 20 m/s responding to four times t=0.65, 1.2, 1.7, and 2.5 s, respectively.

Some information is embedded in Fig. 9a-c, such as the max projectile height H and projectile range R. Taking the solid line (v_0=20 m/s) as an example, in Fig. 9b, the max height of H=4.75 m happens at time 1 s at point y=y_H=4.75, x=x_H=13.58 m (see Fig. 9a), and z=z_H=-8.16 m (see Fig. 9c). The max projectile range R is defined as the distance between the initial point (x_0, y_0, z_0) and landing point (x_R, y_R, z_R). When the ball lands on the ground x-z plane, y_H equals to 0 m. In Fig. 9b, it notes for y_H=0, time t=2 s. In Fig. 9a, for time t=2 s, the max x-projectile range equals the distance between x_0=0 and x_R=24.93 m. In Fig. 9c, for time t=2 s, the max z-projectile range equals the distance between z_0=0 and z_R=-15.46 m. The magnitude of the max projectile range R can be calculated using Equation 4.7.

$$R = \sqrt{(x_R - x_0)^2 + (z_R - z_0)^2} \quad (4.7)$$

In the result that this example can be summarized as: when a soccer ball is kicked to shoot with an initial velocity v_0 =20 m/s at the initial projectile angle θ_0=30°, and initial orientation angle β_0=30°, the max projectile height H=4.75 m happens at the point (13.58, 4.75, -8.16) at time 1 s. And, the max projectile range R=29.33 m does at the point (24.93, 0, -15.46) at time 2 s.

Similarly, the max projectile height H and projectile range R for the initial velocities v_0=5, 10, and 15 m/s can be obtained in Fig. 9a-c. The entire information is listed in Table 1, where some significant kinematics results can be obtained.

Table 1. Max projectile height H and projectile range R for initial velocities v_0=5, 10, 15 and 20 m/s

Initial velocity	Max projectile height			Max projectile range		
1	2	3	4	5	6	7
v_0 (m/s)	H (m)	@ time (s)	@ point (x_H, y_H, z_H) (m)	R (m)	@ time (s)	@ point (x_R, y_R, z_R) (m)
5	0.32	0.26	(0.97,0.32,-0.56)	2.14	0.5	(1.85,0,-1.07)
10	1.25	0.50	(3.65,1.25,-2.13)	8.27	1.0	(7.12,0,-4.20)
15	2.76	0.74	(7.86,2.76,-4.65)	17.64	1.5	(15.1,0,-9.12)
20	4.75	1.00	(13.58,4.75,-8.16)	29.33	2.0	(24.93,0,-15.46)

Result 1: it can find how the max projectile height H or the max projectile range R changes with an initial velocity v_0. Using the data in columns 1 and 2, the relationship between the max projectile height H and initial velocity v_0 is generated in Fig. 10. It notes that H non-linearly increases with the increase of v_0. Also, using the data in columns 1 and 5, the relationship between the max projectile range R and initial velocity v_0 is generated in Fig. 11. Similarly, R increases with the increase of v_0 non-linearly. Therefore, if the initial projectile angle and initial orientation angle keep two independent constants when launching a ball with a series of the initial velocities, the max projectile height H or the max projectile range R non-linearly increases with the increase of initial velocity.

Result 2: it can see how the ball landing points distribute in the x-z ground plane for the initial velocities v_0=5, 10, 15, and 20 m/s. Using the data in columns 5 and 7, the four landing points are plotted in the 3D x-y-z space as shown in Fig. 12. It notes that the four points locate on the x-z ground plane (where y=0). Furthermore, using x_R and z_R data in column 7, the relationship x-z is plotted in Fig. 13. The result indicates that four points are distributed in a straight line for the four initial projectile velocities v_0=5, 10, 15, and 20 m/s when the initial projectile angle θ_0=30°, and initial orientation angle β_0=30°. Therefore, if the initial projectile angle and initial orientation angle keep two independent constants when launching a ball with a series of initial velocities, the landing points show a straight line distribution.

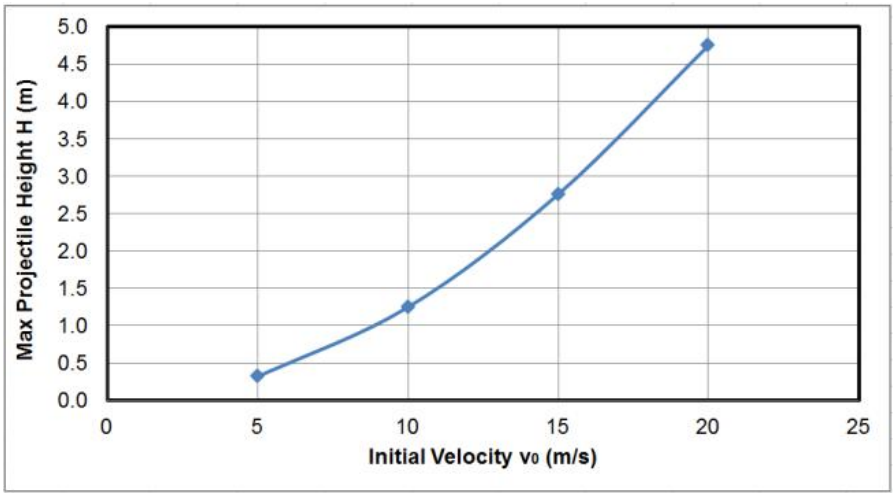

Fig. 10. The relationship between the max projectile height H and initial velocity v_0

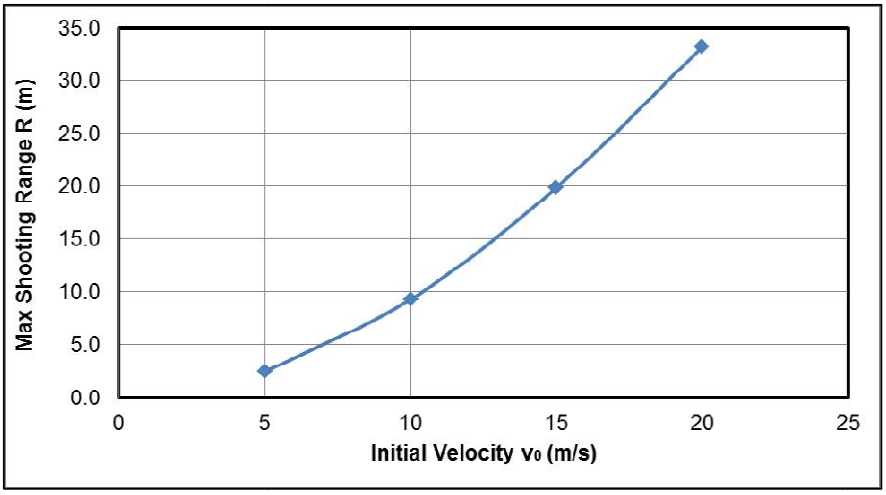

Fig. 11. The relationship between the max projectile range R and initial velocity v_0

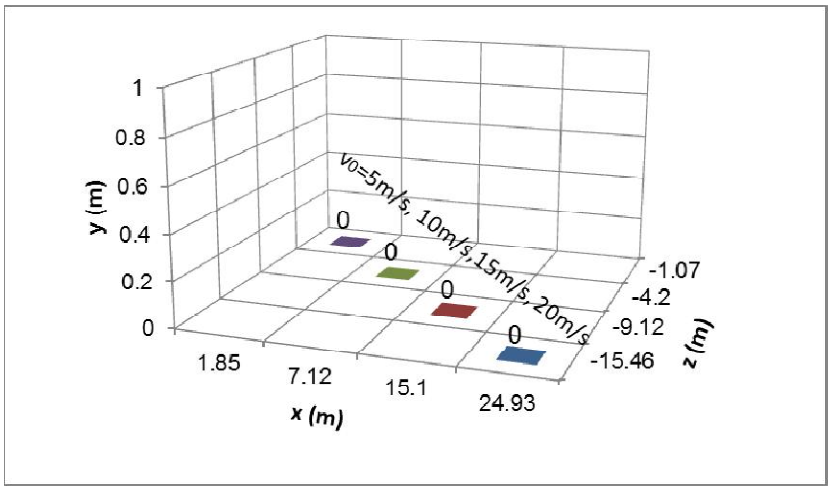

Fig. 12. The distribution of the landing points for four initial projectile velocities v_0= 5, 10, 15 and 20 m/s

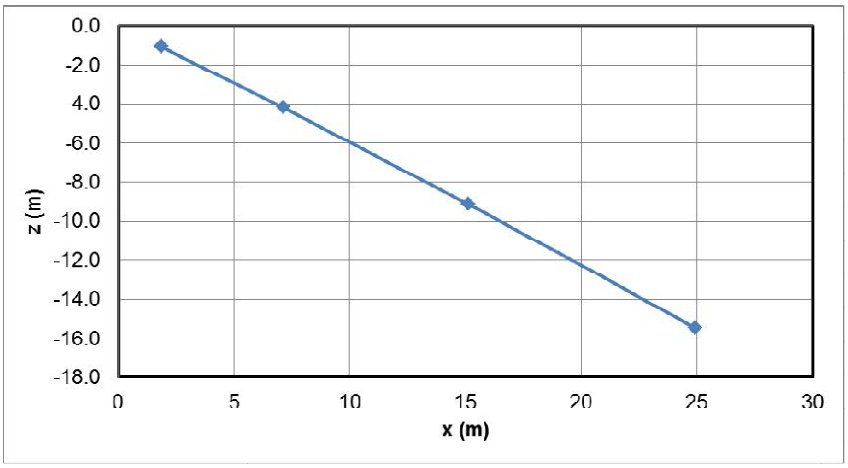

Fig. 13. The relationship of max z-projectile range and the max x-projectile range for four initial projectile velocities v_0= 5, 10, 15 and 20 m/s

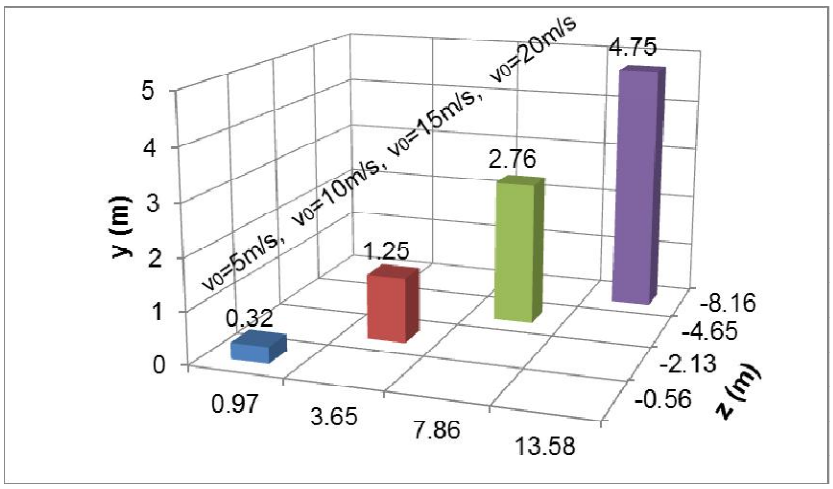

Fig. 14. The distribution of the max projectile height points for four initial projectile velocities v_0= 5, 10, 15 and 20 m/s

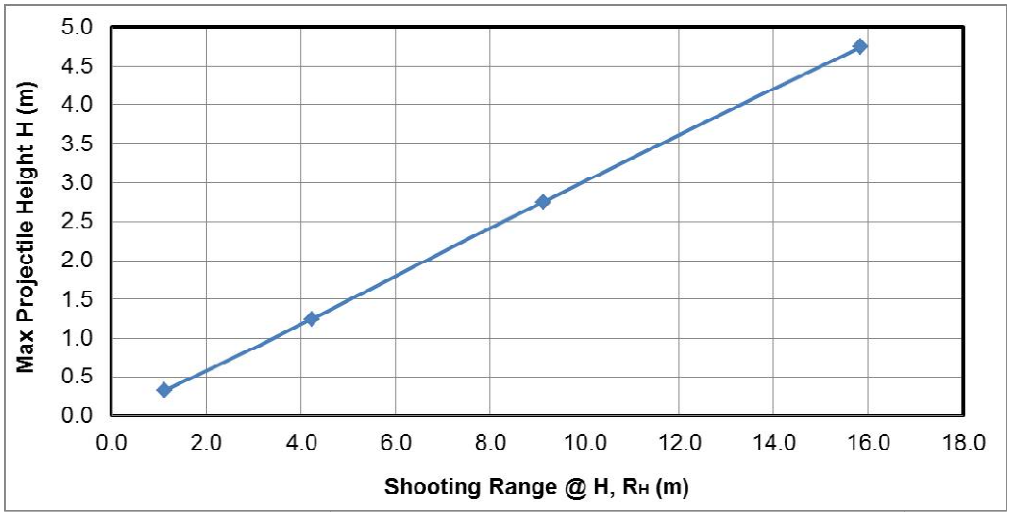

Fig. 15. The relationship of max projectile height H with its projectile range R_H for four initial projectile velocities v_0= 5, 10, 15 and 20 m/s

Result 3: it can find how the max projectile height H changes with its corresponding projectile range R_H for the four initial velocities v_0 =5, 10, 15 and 20 m/s. Using the data in columns 2 and 4, the four points of the max projectile height H are plotted in the coordinate x-y-z as shown in Fig. 14. The projectile range R_H is located on the x-z plane and defined as the distance between the initial point (x_0, z_0) and point (x_H, z_H) as expressed in Equation 4.8.

$$R_H = \sqrt{(x_H - x_0)^2 + (z_H - z_0)^2} \tag{4.8}$$

Substituting x_H and z_H data (see column 4) to Equation 4.7, and then it can get R_H. The relationship H-R_H is plotted in Fig. 15. It notes that the H rises with the rising R_H linearly for four initial projectile velocities v_0 =5, 10, 15, and 20 m/s when the initial projectile angle θ_0=30°, and initial orientation angle β_0=30°. Thus, if the initial projectile angle and initial orientation angle individually keep two constants, when launching a ball with a series of initial velocities, the max height points form a straight line distribution.

4.2 Dynamics Simulation and Analysis

In this case study, some interesting dynamics results can be generated from the simulation and animation of the soccer ball air dynamics, as well as integrating the principle of linear impulse and momentum in the dynamics simulation. The details are discussed in the following two segments.

4.2.1 Soccer ball impulsive force

Continuing the above case study, by integrating the principle of linear impulse and momentum in the dynamics simulation, it can determine how big is the impulsive force applied on the ball for the four initial velocities v_0=5, 10, 15, and 20 m/s. The ball is initially at rest on the ground and is kicked. Fig. 16 shows a diagram of this initial configuration. When the ball leaves the player's foot, the ball travels with initial shooting velocities v_0 at initial projectile angle θ_0=30°, and initial orientation angle β_0=30°. If the foot and ball are in contact with Δt=0.012 s, the magnitude, and direction of the average impulsive force P can be calculated using the principle of linear impulse and momentum as given in Equation 2.1a in Section 2.

Thus, the linear impulse on the ball is equal to the change linear momentum. Substituting $(m\vec{v})_1$=0 and $(m\vec{v})_2$=m$\vec{v}_0$ to Equation 2.1a yields Equation 4.8 for calculating force P.

$$\vec{P} = \frac{m\vec{v}_0}{\Delta t} \tag{4.9}$$

Equation 4.8 builds a linear relationship between the impulsive force P and the initial velocity v_0. Furthermore, the variation of P with v_0 is plotted in Fig. 17. It notes that the force P linearly increases with the increase of the initial velocity v_0. When m=0.43 kg, the magnitude of the average impulsive forces P=107.5, 215.0, 322.5 and 430 N for the four initial velocities v_0=5, 10,

15 and 20 m/s, respectively, at the initial projectile angle $\theta_0=30^o$, and initial orientation angle $\beta_0=30^o$.

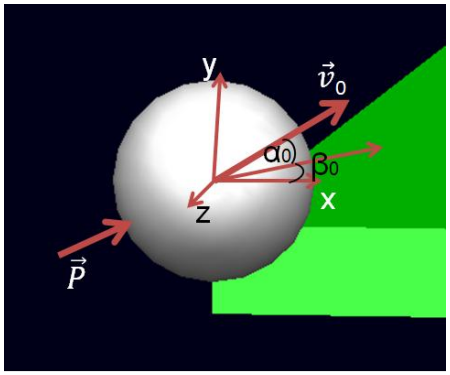

Fig. 16. Initial configuration for the soccer ball projectile motion

4.2.2 Soccer ball air resistance

Fig. 18a-d demonstrates the 3D air resistance-directed graphics of the soccer ball projectile motion with four initial velocities v_0=5, 10, 15 and 20 m/s responding to the times t=0.7, 1.2, 1.7 and 2.5 s, respectively. The numerical resistance distributions, which are embedded in the visualized trajectories, are shown up. The x-y-z components are labeled in the dynamic local coordinate systems, which are attached to trace position points and changes with the time.

Fig. 19a-c plots the air resistance applied on the ball traveling in x-y-z directions with four initial velocities v_0=5, 10, 15 and 20 m/s responding to the times 0.65, 1.2, 1.7 and 2.5 s, respectively. It reveals the distribution of air resistance versus the initial velocity or time.

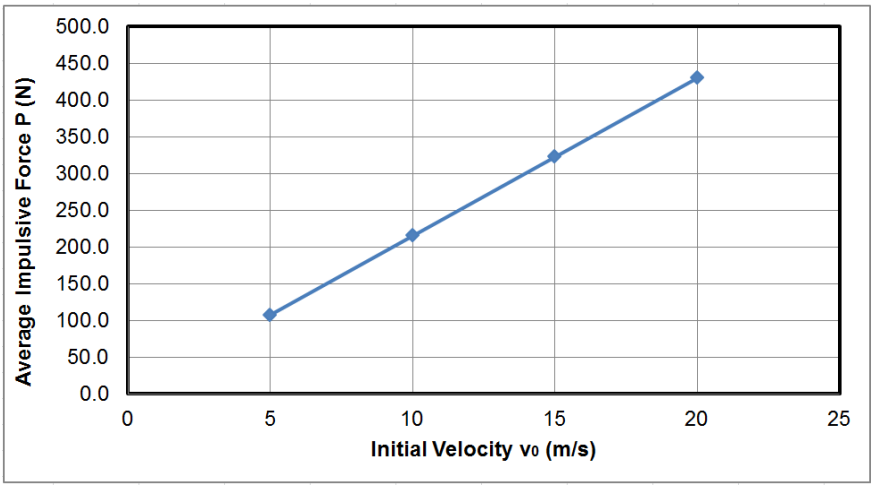

Fig. 17. The variation of the impulsive force P with four initial velocities v_0=5, 10, 15 and 20 m/s

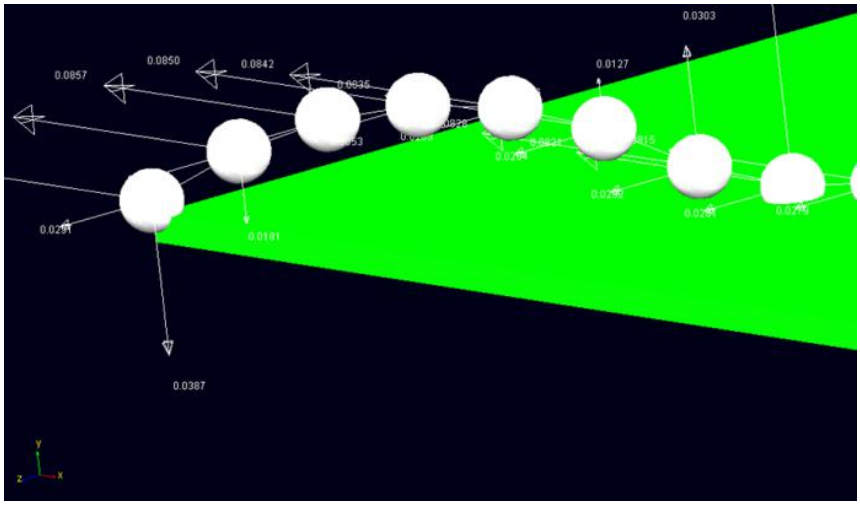

(a) Initial velocity v0=5 m/s

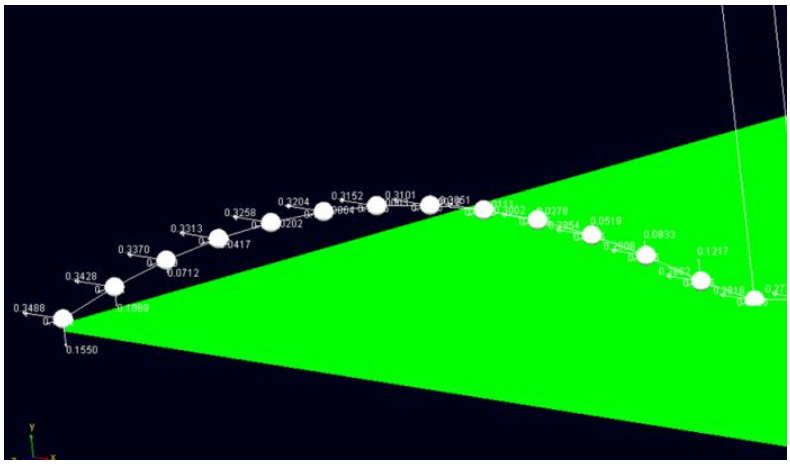

(b) Initial velocity v0=10 m/s

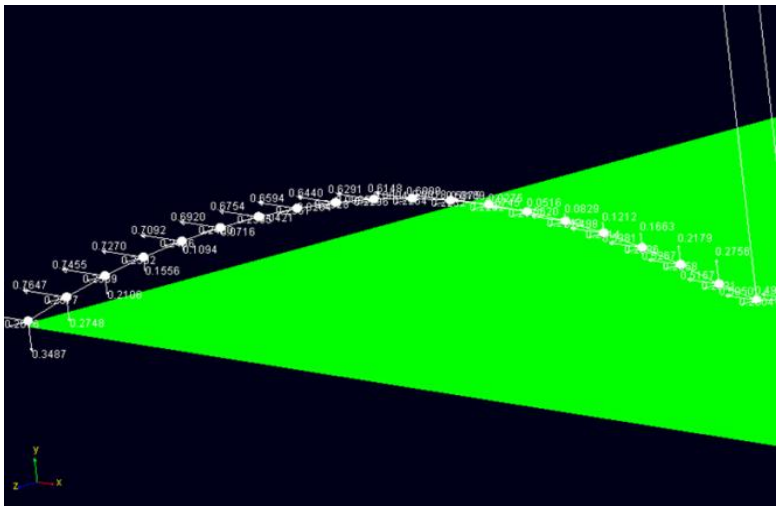

(c) Initial velocity v0=15 m/s

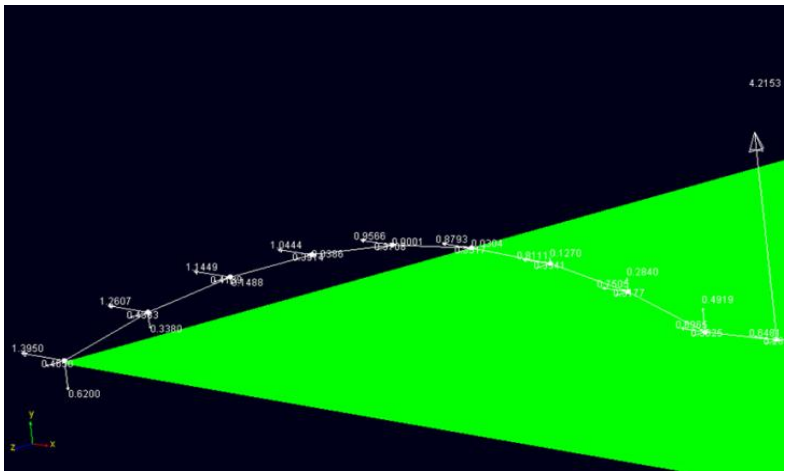

(d) Initial velocity v0=20 m/s

Fig. 18. 3D air resistance-directed graphics of the soccer ball projectile motion with four initial velocities

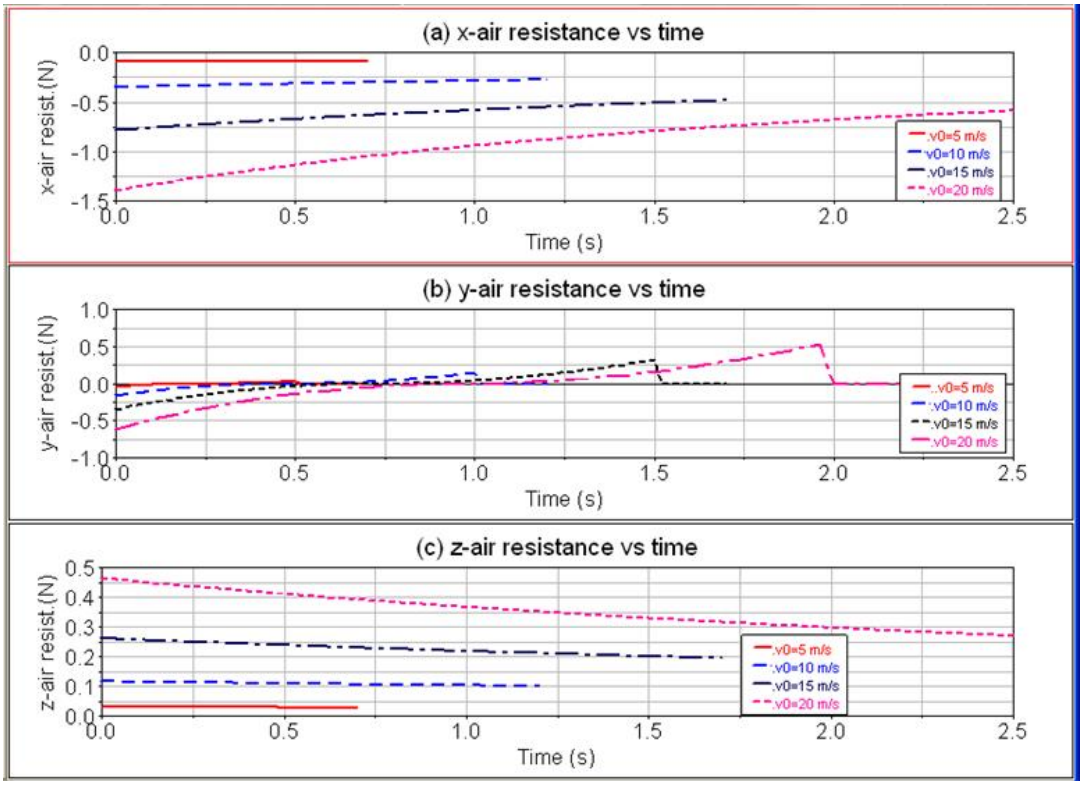

Fig. 19. Air resistance applied on the soccer ball in x-y-z directions with four initial velocities v_0= 5, 10, 15 and 20 m/s

Taking a look at the air resistance along the x-direction as shown in Fig. 19a, for a given time, the resistance magnitude $|F_x|$ increases with the increase of the initial velocity; and for a given trajectory, the air resistance magnitude decreases with the increase of the time. The interpretation of this variation is that, as the ball moves through the air, the air resists the motion of the ball so that the velocity of the ball slows down. Checking Equation 2.7 (F_x=-Kv_x^2) the air resistance F_x is proportional to the squared velocity of the ballv_x^2. Therefore, the resistance magnitude decreases with decreasing velocity.

Fig. 19b shows the four curves of the air resistance-time history along the y-direction. For a given trajectory, the air resistance increases from the lowest value to zero and then increases to the highest value. The interpretation of this variation is that, as the ball moves through the air in the y-direction, the forces applied on the ball involve gravity and air resistance. Before the ball reaches the max projectile height, the gravity and resistance resist the motion of the ball so that the velocity of the ball slows down. Just as mentioned in the above paragraph, the air resistance is proportional to the squared velocity of the ball. Thus, the resistance magnitude decreases with the decreasing velocity until the velocity equals zero. Then, the ball reverses direction and goes down with a velocity, which is increased with time. The resistance still keeps on resisting the motion of the ball and its magnitude increases with increasing velocity.

Moving to Fig. 19c, the curves of air resistance-time along the z-direction have similar trends as along the x-direction. For a given time, the resistance increases with increasing initial velocity; and for a given trajectory, the air resistance decreases with increasing time. The interpretation of this variation is also similar to Fig. 19a, as the ball moves through the air, the air resists the motion of the ball so that the velocity of the ball slows down. Since the air resistance is proportional to the squared velocity of the ball. Hence, the resistance decreases with decreasing velocity.

This case study focuses on the kinematics and dynamics simulation of a soccer ball projectile

motion. Some interesting items are discussed, such as the global influence of initial velocity on the max projectile height and range over a time interval, as well as the global effect of an air resistance force on a ball over a time interval. The impulsive force applied on the soccer ball is addressed for producing an expected initial velocity.

5. DISCUSSION

Comparing to many published works (see literature review in Introduction), the main contribution of this study can be summarized to the following points.

1. A spatial kinematics and dynamics model of a soccer ball is developed. The model allows randomly applying a kick force or initial velocity on the ball in 3D space. At this point, similar work has published by Zhu et al. [16]. They have designed a training system to simulate the free kick of a soccer ball. The trajectory can be predicted for the given initial parameters. However, the work has focused on the kinematics simulation rather than the dynamics simulation. Therefore, the dynamic contact force of ball-ground doesn't include in their model.
2. In addition to the air resistance, the equation of the contact force between the ball and ground is integrated into the model. The most researches have paid attention to modeling the air resistance on the ball model without the contact force item.
3. The model is validated by the comparison of this simulation result and a theoretical calculation result [8]. The most theoretical studies do not include model validation. Actually, it is very important to verify if the model is reliable to provide the exact simulation results.
4. The instantaneous force applied to the ball is visualized and plotted with the simulating time, which is useful to analyze the dynamic performance. There are a lot of studies about flight trajectories. But, it is hard to find the distribution of dynamic forces.
5. Using an example to introduce the model application as well as kinematics and dynamics analysis. The purpose of this study is the sports analysis. Therefore, the detailed result analysis and discussion are emphasized. The most previous studies have focused on the development of a simulation system, but have not performed a detailed analysis and discussion of the simulation results.

6. CONCLUSIONS

A spatial dynamic model of a soccer ball has been proposed to perform the kinematics and dynamics simulation for efficient sports analysis. The general model is composed of the three sub-models: (1) impulsive force model, (2) projectile motion model, and (3) ball-ground contact model. Sub-model 1 has been built to calculate the kick force and initial velocity employing the principle of linear impulse and momentum. Sub-model 2 has been established to generate the ball motion and air resistance applied on the ball using Newton's section law and aerodynamics. Sub-model 3 has been created as a mass-spring-dashpot system to compute the contact force between the ball and ground.

The simulation has focused on the animation outputs to visualize the soccer ball projectile motion trajectory with instantaneous air resistance information; and numerical outputs to present the time-varying impulsive force of the foot-ball, projectile motion (displacements, velocities, accelerations), and contact forces of the ball-ground. The model validation is conducted by the comparison of this simulation result and a theoretical calculation result [8]. A good agreement has been obtained between the two models.

An example is given to indicate the kinematics and dynamics simulation of a soccer ball projectile motion in a virtual environment. In kinematics simulation & analysis, the influences of initial velocity on the time-related projectile height and range have been analyzed and discussed. In dynamics simulation & analysis, the effects of air resistance force on a traveling ball over a time interval have been investigated and studied. The impulsive force applied on the soccer ball has been discovered for producing an expected initial velocity. Bringing the above work together forms a complete procedure for the case study to illustrate the application of dynamic simulation on soccer ball projectile motion analysis.

This research is significant to model, simulate, and analyze the soccer ball motion for optimizing trajectory and accurate position.

Three aspects require to be improved through further investigation. They are: (1) model improvement, such as extending the current equations of motion by adding some factors of soccer ball flying spin, Magnus effect, and gyroscopic moment; (2) validation extension, such as taking experimental means to obtain testing data, and then compare experimental results with the simulated results; and (3) case-study diversification, such as performing the case studies with unsteady-state airflow for further illustrate the kinematics and dynamics simulation.

COMPETING INTERESTS

Authors have declared that no competing interests exist.

REFERENCES

1. Meriam JL, Kraige LG. Engineering mechanics, dynamics, 5th edition. Wiley, John & Sons, Incorporated, New York, USA; 2002.
2. Sokolnikoff IS, Sokolnikoff ES. Higher mathematics for engineer and physicists. McGraw Hill Book Company, Inc., New York, USA; 1941.
3. MSC Software. Automatic dynamic analysis of mechanical systems. Technic Manual, University of Michigan, USA; 2004.
4. Goff JE, Carré MJ. Trajectory analysis of a soccer ball. Am J Phys. 208;77:1020–1027.
5. Gupta G, Panigrahi PK. Curve kick aerodynamics of a soccer ball. Proceeding of the Fortieth National Conference on Fluid Mechanics and Fluid Power, Himachal Pradesh; 2013.
6. Asai T, Seo K, Kobayashi O, Sakashita R. Fundamental aerodynamics of the soccer ball. Sports Engineering. 2007;10:101–109.
7. Asai T, Seo K. Aerodynamic drag of modern soccer balls. SpringerPlus. 2013; 2:171.
8. Bray K and Kerwin DG. Modelling the flight of a soccer ball in a direct free kick.J Sports Sci. 2003;21:75–85.
9. NASA. Drag on a Soccer Ball. National Aeronautics and Space Administration Technic Paper; 2018.
   Available: www.nasa.gov
10. Hroncová D, Grieš M. Trajectories of projectiles launched at different elevation angles and modify design variable in MSC Adams/View. Applied Mechanics and Materials. 2014;611:198-207.
    [ISSN: 1662-7482]
11. Alam F, Chowdhury H, Moria H. A comparative study of football aerodynamics. J. Procedia Eng. 2010;2: 2443–2448.
12. Alam F, Ho H, Chowdhury H. and Subic A. Aerodynamics of baseball. J. Procedia Eng. 2011;13: 207–212.
13. Zhu ZQ, Chen B, Qiu SH, Wang RX. Simulation and modeling of free kicks in football game and and anslysis on assisted training. Asia Sim. 2017;413-427. Part I, CCIS751.
14. Smith MR, Hilton DK, Van Sciver SW. Observed drag crisis on a sphere in flowing He I and He II, Phys. Fluids. 1999; 11:751–753.
15. Synge JL, Griffith BA. Principles of mechanics. McGraw Hill, New York; 1959.
16. Thomson WT. Theory of vibrations with applications, 4th ed., Prentice-Hall, New York; 1993.

Peer-review history:
The peer review history for this paper can be accessed here:
http://www.sdiarticle4.com/review-history/53390